ADVANCED MATERIALS
www.advmat.de

Materials Views
www.MaterialsViews.com

COMMUNICATION

Powerful, Multifunctional Torsional Micromuscles Activated by Phase Transition

*Kai Liu, Chun Cheng, Joonki Suh, Robert Tang-Kong, Deyi Fu, Sangwook Lee, Jian Zhou, Leon O. Chua, and Junqiao Wu**

Miniaturisation of conventional rotary motors is a great challenge because of their complex design, especially if robust and diverse functionalities are to be integrated inside a very limited space. Piezoelectric ultrasonic micro-motor is a successful alternative although its size is still on the millimetre scale.[1] Further scaling down requires to pursue different designs with judiciously chosen active materials to deliver powerful outputs. Although an electrostatically driven microelectromechanical motor was developed twenty years ago,[2] its inherently on-chip structure complicates the integration to drive other devices. Similar mechanism was used to develop carbon nanotube based nanoelectromechanical actuators.[3] Rotary magnetic field was also utilized to actuate the rotation of micro magnetic metal paddles.[4] Torsional muscles using sole or guest-filled twisted carbon nanotube yarns were recently reported.[5,6] These micro or nanoscale motors and actuators, however, all deliver a single function, i.e., torsional motion. For micro-robots in simulation of living organisms, it is much desired to have a micro torsional muscle integrating multifunctions in a limited space, such as simultaneous actuation and sensing. In addition, higher power density, larger rotation amplitude, and higher rotational speed are indispensable requirements in these applications.

VO_2 emerges as an ideal driving material for multifunctional artificial muscles, owing to its simultaneously high Young's modulus (~140 GPa), high transformation strain (1~2% in single crystals), and intrinsically fast speed (~picosecond) in its metal-insulator transition (MIT) at ~68 °C.[7,8] Its volumetric work density is up to 7 J/cm^3 for single-crystal nanowires,[9] which is two orders of magnitude higher than piezoceramics[10] and 3 orders higher than human muscles.[11] Although VO_2 based linear and bending actuators have been demonstrated,[9,12–18] development of torsional ones is still a great challenge. Here we demonstrate a set of micro bimorph coils that function as powerful torsional muscles, driven thermally or electrothermally by a metal-insulator phase transition in the active material, vanadium dioxide thin films (volumetric work density ~0.6 J/cm^3). Reversible torsional motion over one million cycles without degradation is demonstrated, with a superior rotational speed up to ~200 000 rpm, amplitude of 500° per mm length, and power density up to ~39 kW/kg. These torsional muscles combine multiple functions as torsional actuators, micro catapults, proximity sensors, as well as memristors. Being able to sense a distanced object and then respond by rotating to a different configuration, the torsional muscles simulate active neuromuscular systems with all-inorganic materials.

The micro torsional muscle was fabricated by releasing a long "V"-shaped Cr/VO_2 bimorph structure. VO_2 thin films were first grown by pulsed laser deposition on Si substrates with a 1.1 μm thick thermal oxide. The "V"-shaped Cr pattern was lithographically defined and deposited onto the VO_2 layer, followed by an anneal process (**Figure 1**a). Afterwards, the unprotected area of VO_2 was etched away by reactive ion etching (RIE). Then the "V"-shaped Cr/VO_2 area was covered by photoresist with the same pattern, and the exposed SiO_2 and the underneath Si were deep-etched to a depth of ~25 μm, both by deep RIE (Figure 1b). Finally, the photoresist was removed, and the SiO_2 layer beneath the Cr/VO_2 was under-etched by buffered oxide etchant, releasing the "V"-shaped Cr/VO_2 bimorph ribbon (Figure 1c).

The resultant structure is a suspended bimorph helix consisting of two symmetric coils (thereafter termed as a "dual coil") naturally connected to the two Cr electrode pads, with a size of tens to hundreds of micrometres, as shown in Figure 1d-f. The initial curvature originates from the stress built in the metal deposition and anneal process.[9] The coil axial length and coil ribbon length of the structure are given by the distance between the two electrode pads and the arm length of the "V"-shaped structure, respectively (Figure 1d-f). It is possible to further reduce the size of coils. The thickness of VO_2 and Cr layer can be further reduced down to several to tens of nanometers. At these thicknesses the VO_2 thin film is expected to still retain the phase transition to drive the actuation (this is a great benefit compared to shape memory alloys which would lose the memory functionality at these thicknesses), and the coil would form at smaller diameters (Figures 1d-f and Figure S1). The diameter can be further reduced by increasing the annealing temperature to improve the inter-layer bonding.[9] By these efforts, a device with a size of several to tens of micrometers or even smaller is possible. The challenge is purely technical and lies in the fabrication process, because these ultrathin films may be difficult to survive the dry and wet etching steps.

Dr. K. Liu, Dr. C. Cheng, J. Suh, Dr. D. Fu, Dr. S. Lee,
J. Zhou, Prof. J. Wu
Department of Materials Science and Engineering
University of California
Berkeley, California 94720, USA
and Materials Sciences Division
Lawrence Berkeley National Laboratory
Berkeley, California, 94720, USA
E-mail: wuj@berkeley.edu

R. Tang-Kong, Prof. L. O. Chua
Department of Electrical Engineering and Computer Sciences
University of California
Berkeley, California
94720, USA

DOI: 10.1002/adma.201304064

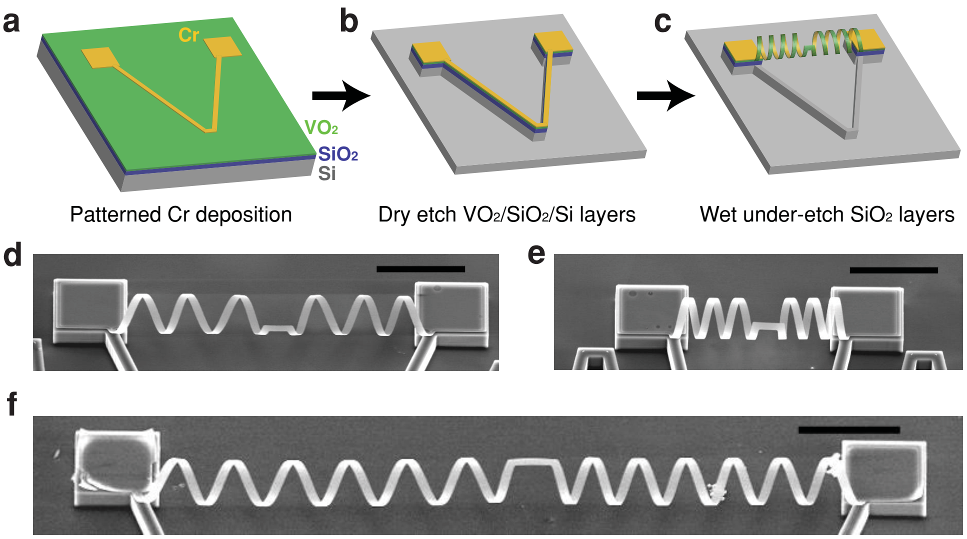

Figure 1. Fabrication of VO_2-based bimorph coils. a-c) Schematic of the microfabrication process. d-f) SEM images of bimorph coils with different coil lengths. The bimorphs consist of 30 nm thick Cr and 150 nm thick VO_2 with a total coil length of 1 mm (d, e) and 2 mm (f). Scale bars are 100 μm.

The as-fabricated dual coil can be actuated by increasing the temperature of the entire chip (global heating), but more conveniently, by Joule heating of current flowing through the coil itself. Such electrical control of actuation allows addressing individual devices at much higher speed than by global heating. The parallel connection of the VO_2 and Cr layers offers a good electrical conduction and therefore a low work voltage. Movie S1 shows a dual coil rotating under an applied sine-wave voltage. As temperature rises with the increase of current, the curvature of the coil drops drastically by the phase transition of VO_2, and the coil is untwisted providing a torsional actuation. **Figure 2**a shows a dual coil rotating to its maximum amplitude under an input voltage of 3.1 V, where the input power is only ~3 mW. When the driving voltage slowly varies, the coil switches between a high-resistance state corresponding to the insulating phase of VO_2, and a low-resistance one corresponding to its metallic phase (Figure 2b). The hysteresis between the forward and backward sweeping results from the intrinsic supercooling and superheating of the phase transition in VO_2.[19] All of the current-voltage curves go through the origin regardless of the sweeping frequency (inset of Figure 2b). The area enclosed by the current-voltage loop increases initially as a function of the sweeping frequency, then decreases monotonically after ~100 Hz, and eventually converges to a straight line obeying the Ohm's law. These are the fingerprints of a memristor,[20,21] akin to the memristor behaviour of sodium and potassium ion channels,[22] implying potential applications in neuron-mimetic devices.[22,23] Combined with the structural actuation, these devices may also lead to implementation of mem-inductors and mem-capacitors.[24]

Driving the dual coil with a square-wave input voltage reveals the high speed of actuation (Movie S2). In ambient air, the response time, defined as the time that the coil takes to respond from 10 to 90% of the step height of resistance, is 0.54 ms and 0.26 ms in the switch-on and switch-off step, respectively (Figure 2c). Thus the maximum response frequency for a cycle of rotation is ~1200 Hz in air (in liquid, it is ~50 Hz, see Figure S2). The shorter switch-off time, which is opposite to the result shown in photo-thermal actuation,[15] is not only due to the the boundary condition of heat transfer to the substrate through the two metal pads, but also attributed to the very thin bimorph ribbon (<200 nm in thickness) with large surface area that allow the heat to dissipate into air more quickly in the cooling cycle.

The fast response in resistance raises a concern of whether the mechanical rotation of a dual coil follows its resistance change. The change of resistance stands for the electronic phase transition of VO_2, while the mechanical motion, which is determined by the lattice phase transition, may not occur at the same speed. Direct measurement of mechanical motion is usually required to clarify this. The rotation amplitude of the same device shown in Figure 2a was measured at various working frequencies. As shown in Figure S3, the rotation shows a 3dB-cut-off frequency (amplitude/$\sqrt{2}$) of ~1 kHz. This cut-off frequency of rotation agrees with the measured cut-off frequency of electrical resistance, which indicates that indeed the electrical transition synchronizes with the mechanical rotation.

The rotation amplitude of the dual coil normalized by the coil axial length is ~2000°/mm, and by the coil ribbon length is ~500°/mm. This specific amplitude is reduced by half from that of a single coil as shown in **Figure 3**a, but the torque is enhanced by a factor of two. The dual coil ribbon length-normalized rotational speed is up to ~600000°/s, or 100000 rpm, per millimetre of ribbon length. For the dual coil with a coil ribbon length of 2 mm (Figure 1f), the rotational speed is ~200000 rpm. This value is 15~300 times higher than that of carbon nanotube based torsional muscles,[5,6] and 1–2 orders of magnitude higher than commercial heat engines and electric motors, as well as ultrasonic motors, as compared in Figure 2e.

The device was driven by a 100 Hz square-wave voltage for one million cycles in ambient air (Figure 2d); afterwards both the rotation amplitude and resistance switch show no noticeable degradation, testifying the mechanical and electrical reliability of the device operation. The maximum torque of a dual

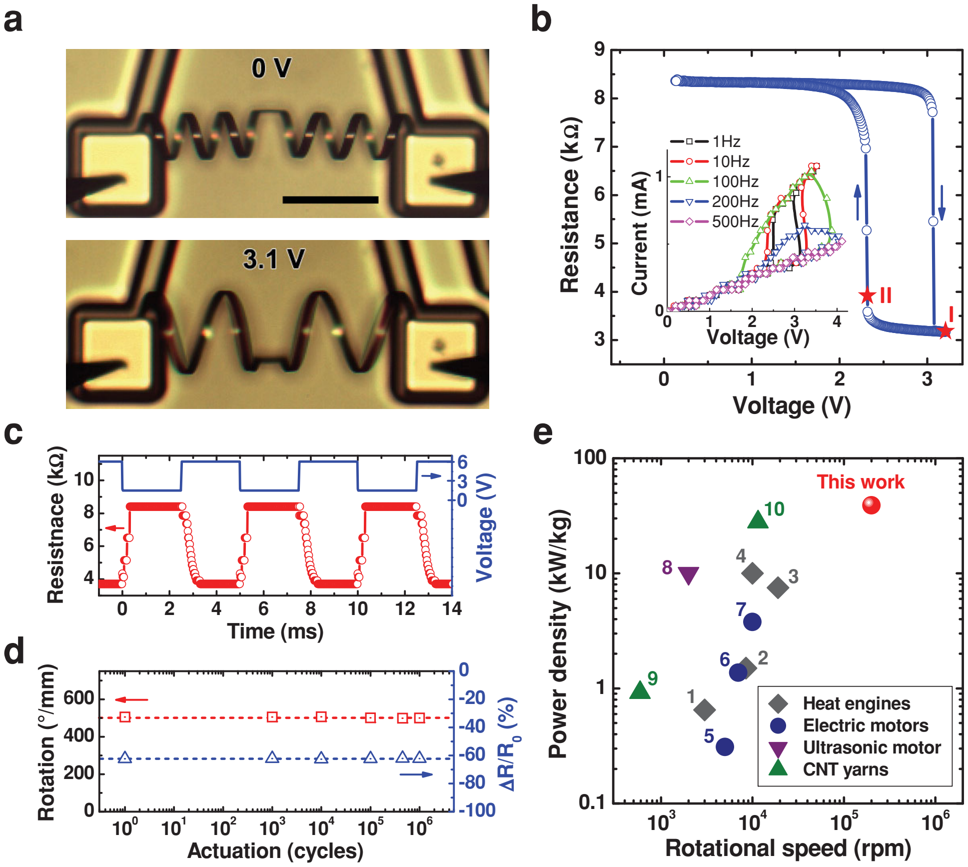

Figure 2. Electrical actuation of dual coils. a) Geometry of a dual coil actuated at 0 V and 3.1 V. Scale bar is 100 μm. b) DC resistance of the coil as a function of driving voltage. The two stars I and II indicate the metallic phase state and phase transition state of VO_2, respectively, utilized for the proximity sensor application. The inset shows its current – voltage characteristic at various frequencies. c) Resistance of the coil driven by a 200-Hz square-wave voltage. d) Endurance test of the torsional actuation, showing robust performance after 10^6 cycles of switch between driving voltages of 0 V and 3.1 V. e) Comparison of the VO_2-based torsional actuation with existing macro to micro scale engines. These are large heat engines (1, Duramax LMM V8 Turbo Diesel for trucks; 2, Mazda 13B-MSP Renesis 1.3 L Wankel for sports cars; 3, BMW V10 3L P84/5 2005 gas Otto for racing cars; 4, GE90–115B Brayton turbofan for Boeing 777), electric motors (5, Panasonic MSMA202S1G AC servo motor; 6, Toyota Brushless AC Nd Fe B PM motor; 7, Himax HC6332–250 Brushless DC motor), small ultrasonic motors (8, see Ref.[1]), and microscale CNT yarn torsional muscles (9, see Ref.[5]; 10, see Ref.[6]).

coil shown in Figure 2a is estimated to be 13.6 pN·m, which is ~1.5 N·m/kg for the coil mass of the device (see Supporting Information for calculation and experimental details). Considering a rotation of 1.4 rounds in a full actuation time of ~0.34 ms of a switch-off step (Figure 2c, extracted from 0 to 100% of the step height of resistance), the peak power density is ~39 kW/kg. This is ~200 times higher than that of mammalian skeletal muscles,[11] several to a hundred of times higher than piezoelectric ultrasonic motors, heat engines, and electric motors, and also surpasses that of the recently developed hybrid carbon nanotube yarn muscles.[5,6]

Unlike electrostatically driven micro-motors, the actuation function is built upon the internal phase transition of the active material, as opposed to interactions between different device components. The resultant benefit is that the structure can be conveniently removed from the fabrication substrate as an off-chip device without losing the functionalities. Figure 3a shows a single coil transferred onto the edge of another substrate being actuated by global heating (also see Movie S3), in which the curvature changes (Figure 3b). The rotational angle amplitude, θ, is given by $360^\circ \cdot \frac{L}{2\pi}\left(\frac{1}{R_i}-\frac{1}{R_f}\right)$, where L is the total coil ribbon length, R_i is the initial radius, R_f is the final radius, and $\frac{1}{R_i}-\frac{1}{R_f}$ is the total curvature change. The specific rotation amplitude of ~1000°/mm (Figure 3c) is four times that of carbon nanotube yarn based torsional muscles,[5] and over three orders of magnitude higher than those achieved in torsional actuators based on shape memory alloys,[25] piezoelectric materials,[26] and conducting polymers,[27] which typically generate torsion on the order of 0.01–0.1°/mm. The high rotation performance benefits fundamentally from the high transformation strain of VO_2 across the MIT. The strain in the bimorph is about –0.3% across the phase transition (Figure 3b), and therefore, ignoring the very small thermal expansion, it gives a high work density of ~0.6 J/cm^3 for the active layer of VO_2 thin film, which is comparable to the reported values of VO_2-based actuators (0.63 J/cm^3 in Reference[9] and 0.81 J/cm^3 in Reference[17]). A bimorph structure usually achieves several to tens of times lower work density depending on the thicknesses of bimorph layers. We roughly estimate the work density of the bimorph dual coil shown in Figure 2a. The torsional work that the coil

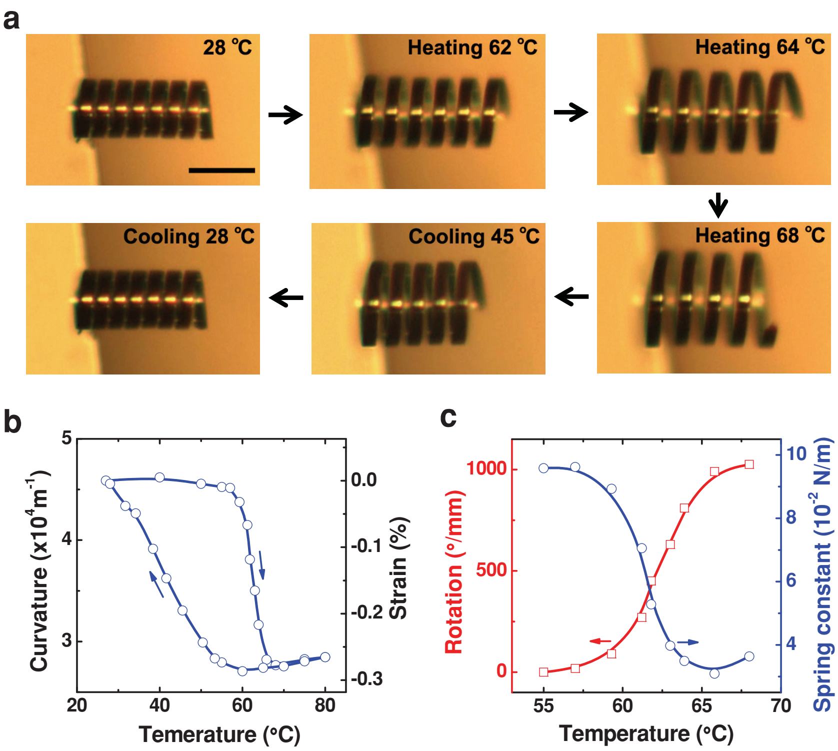

Figure 3. Structural performance of a single coil. a) Rotation of the coil at various temperatures in a heating – cooling cycle. Scale bar is 50 µm. b) Temperature dependence of curvature and strain of the coil. c) Temperature dependence of specific rotation and spring constant in the heating half-cycle.

can output is roughly equal to $\frac{1}{2}T_m\theta_m$, where $T_m = 13.6$ pN·m is the maximum torque and $\theta_m = 1.4 \times 2\pi$ is the maximum rotation, if assuming a harmonic restoration mechanics. Considering the size of the bimorph coil (1 mm (length) × 10 µm (width) × 180 nm (thickness)), the volumetric work/energy density then equals ~0.033 J/cm^3, which is about an order of magnitude lower than the reported value of the VO_2 active layer as the upper limit.

We note that treating the coil as an elastic spring, its spring constant also varies with the change in geometry. From elastic theory[28,29] we calculated the spring constant for the bimorph coil (see Supporting Information for calculation details) and plotted in Figure 3c as a function of temperature. With the MIT occurring in the coil, the spring constant for the coil is reduced by about 2/3, from 0.096 N/m at 55 °C to 0.031 N/m at 66 °C. The tunability in spring constant can be further widened by optimizing the width and thickness of the Cr/VO_2 bimorph as well as the coil length.

With the high level of power density, the coil can function as a powerful apparatus for output of mechanical energy. **Figure 4**a shows that a dual coil holds a micro object in the middle (left panel), and then works as a micro catapult during the rapid actuation to throw out the object (right panel). The weight and size of the object is on the order of ~0.4 µg and ~50 µm, and the throw distance is ~1 mm. The torsional actuator therefore catapults a weight ~50 times heavier than itself for a distance of ~5 times longer than itself, in a period of time shorter than 60 ms (limited by the frame rate of our camera, see Movie S4). The other way to output mechanical energy is through the expansion of the enclosed volume of the coil. With the increase of diameter during the actuation, the volume of the coil rapidly increases by 2 to 3 times in ~1 ms, capable of pushing outward heavy objects surrounding it (Movie S4).

Besides the powerful mechanical function, VO_2 is also an electrically and optically active material responding sensitively to environment temperature, which provides the coil with additional sensing functions. Figure 4b demonstrates a non-contact micro proximity sensor, where the coil is heated by Joule heating. Proximity to a room-temperature micro-object slightly reduces local temperature of the coil; the coil senses the distance, d_s, by changing its resistance. Figure 4c shows the resistance of a proximity sensor

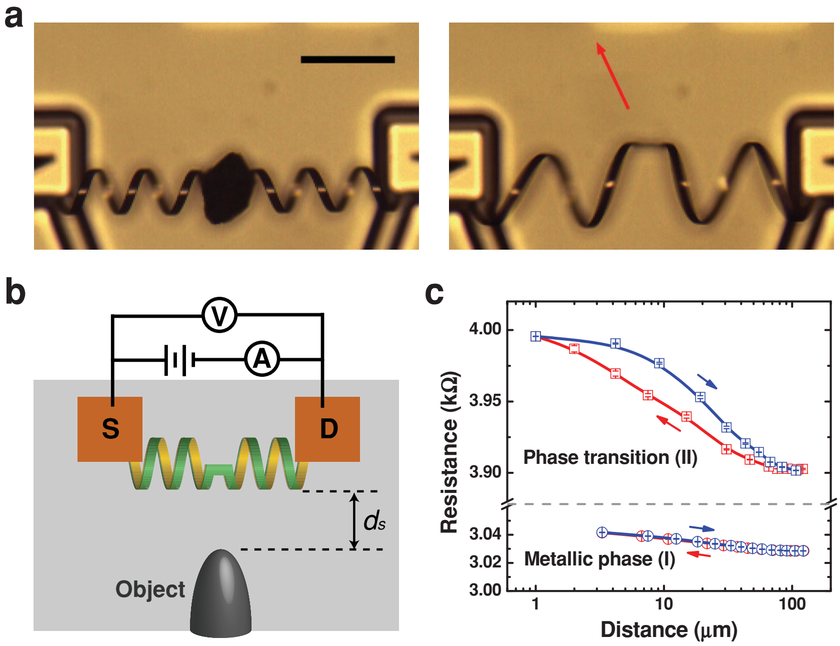

Figure 4. Multifunctionality: micro catapult and proximity sensor. (a) A dual coil as a catapult throwing out a micro object. Scale bar, 100 µm. (b) Schematic of a proximity sensor made of a dual coil. (c) The proximity sensor detects the distance of a room-temperature object (in this case a tungsten tip with a tip diameter of 12 µm). The sensor works at the metallic-phase stage (I) at constant voltage = 3.1 V, or the phase-transition stage (II) at constant current = 0.6 mA, as marked in Figure 2b.

working in a wide distance range of 1–100 µm, at the two phases in the I-V curve shown in Figure 2b. The resistance of the coil sensor changes by only ~0.4% in the purely metallic phase. In contrast, the sensitivity is much higher for the device working in the phase transition regime, with a resistance change of ~2.5%, but with a small hysteresis.

The naturally combined functions of proximity sensing and torsional motion allow the device to remotely detect a target and respond by reconfiguring itself to a different shape. This simulates living bodies where muscles and neurons work together to deliver the full activity: neurons sense and deliver stimuli to the muscles and the muscles provide motion. Considering the built-in memristive behaviour, it is also possible to simulate active learning process with the devices.[30]

In summary, we demonstrate a micro torsional muscle driven by the phase transition of VO_2, with a simple design but superior performance in power density, rotation amplitude, and rotational speed. The artificial muscle also combines all the functions including torsional actuator, memristor, and proximity sensor, showing great potential in applications that require a high level of functionality integration in a small space.

Experimental Section

Microfabrication of Bimorph Coil: VO_2 thin films were grown by pulsed laser deposition on 1.1 µm thick SiO_2/450 µm thick Si substrates, at a laser intensity of 2 J/cm^2, growth temperature of 520 °C, and oxygen pressure of 10 mTorr. "V"-shaped Cr pattern was defined on VO_2 thin films by photolithography, e-beam evaporation, and lift-off process. Annealing was carried out at 300 °C for 2 min in a rapid thermal annealing furnace under Ar environment. VO_2 was etched by RIE in a mixed gas of SF_6 (90%) and O_2 (10%), under a pressure of ~90 mTorr, at a working power of 100 W, and with an etch rate of ~20 nm/s. SiO_2 was deep etched by C_4F_8/H_2 (15/8 sccm) at 4 mTorr under a bias power of 350W, with an etch rate of ~0.3 µm/min. Si was deep etched through a Bosch process in which SF_6/O_2 (130/13 sccm, 35 mTorr, 10s) and C_4F_8 (80 sccm, 18 mTorr, 7s) were switched regularly for etch and passivation, with an etch rate of ~2 µm/min. The under-etch of SiO_2 was realized through buffered oxide etchant (BOE 5:1), with an etch rate of ~100 nm/min.

Measurement Specifics: The torsional coil was thermally actuated on a heating stage at a heating/cooling rate of 5 °C/min. The cycled electrical actuation was driven by an Agilent 33250A generator, with square-wave, sine-wave, and ramp-wave signals. To measure the temporal response of a torsional coil, a reference resistor was connected in series with the torsional coil, and the voltage drop on the resistor was recorded by an oscilloscope (Tektronix TBS2000), which is proportional to the current in the circuit. The micro objects used in the throwing and pushing experiments were Si_3N_4 particles obtained from standard sandpapers.

Supporting Information

Supporting Information is available from the Wiley Online Library or from the author.

Acknowledgements

This work was supported by the U.S. Department of Energy Early Career Award DE-FG02–11ER46796. Some of the measurements and materials processing used facilities in the Lawrence Berkeley National Laboratory, which was supported by the Office of Science, Office of Basic Energy Sciences, of the U.S. Department of Energy under Contract No. DE-AC02–05CH11231. Part of work was supported by the AFOSR grant FA 9550-13-1-0136. We thank Prof. R. Ramesh for support of the pulsed laser deposition.

Received: August 13, 2013
Revised: October 30, 2013

[1] K. Uchino, *Smart Mater. Struct.* **1998**, *7*, 273.
[2] Y.-C. Tai, R. S. Muller, *Sens. Actuators* **1989**, *20*, 49.
[3] A. M. Fennimore, T. D. Yuzvinsky, W.-Q. Han, M. S. Fuhrer, J. Cumings, A. Zettl, *Nature* **2003**, *424*, 408.
[4] L. Zhang, J. J. Abbott, L. Dong, K. E. Peyer, B. E. Kratochvil, H. Zhang, C. Bergeles, B. J. Nelson, *Nano Lett.* **2009**, *9*, 3663.
[5] J. Foroughi, G. M. Spinks, G. G. Wallace, J. Oh, M. E. Kozlov, S. Fang, T. Mirfakhrai, J. D. W. Madden, M. K. Shin, S. J. Kim, R. H. Baughman, *Science* **2011**, *334*, 494.
[6] M. D. Lima, N. Li, M. Jung de Andrade, S. Fang, J. Oh, G. M. Spinks, M. E. Kozlov, C. S. Haines, D. Suh, J. Foroughi, S. J. Kim, Y. Chen, T. Ware, M. K. Shin, L. D. Machado, A. F. Fonseca, J. D. Madden, W. E. Voit, D. S. Galvao, R. H. Baughman, *Science* **2012**, *338*, 928.
[7] J. Cao, E. Ertekin, V. Srinivasan, W. Fan, S. Huang, H. Zheng, J. W. L. Yim, D. R. Khanal, D. F. Ogletree, J. C. Grossman, J. Wu, *Nature Nanotech.* **2009**, *4*, 732.
[8] S. Wall, D. Wegkamp, L. Foglia, K. Appavoo, J. Nag, R. F. Haglund, J. Stähler, M. Wolf, *Nat. Commun.* **2012**, *3*, 721.
[9] K. Liu, C. Cheng, Z. Cheng, K. Wang, R. Ramesh, J. Wu, *Nano Lett.* **2012**, *12*, 6302.
[10] R. J. Wood, E. Steltz, R. S. Fearing, *Sens. Actuators A: Physical* **2005**, *119*, 476.
[11] T. Mirfakhrai, J. Madden, R. Baughman, *Mater. Today* **2007**, *10*, 30.
[12] A. Rúa, F. l. E. Fernández, N. Sepúlveda, *J. Appl. Phys.* **2010**, *107*, 074506.
[13] J. Cao, W. Fan, Q. Zhou, E. Sheu, A. Liu, C. Barrett, J. Wu, *J. Appl. Phys.* **2010**, *108*, 083538.
[14] A. Tselev, J. D. Budai, E. Strelcov, J. Z. Tischler, A. Kolmakov, S. V. Kalinin, *Nano Lett.* **2011**, *11*, 3065.
[15] R. Cabrera, E. Merced, N. Sepúlveda, F. l. E. Fernández, *J. Appl. Phys.* **2011**, *110*, 094510.
[16] E. Merced, N. Dávila, D. Torres, R. Cabrera, F. E. Fernández, N. Sepu?lveda, *Smart Mater. Struct.* **2012**, *21*, 105009.
[17] E. Merced, X. Tan, N. Sepúlveda, *Sens. Actuators A - Phys.* **2013**, *196*, 30.
[18] K. Wang, C. Cheng, E. Cardona, J. Guan, K. Liu, J. Wu, *Acs Nano* **2013**, *7*, 2266.
[19] W. Fan, J. Cao, J. Seidel, Y. Gu, J. W. Yim, C. Barrett, K. M. Yu, J. Ji, R. Ramesh, L. Q. Chen, J. Wu, *Phys. Rev. B* **2011**, *83*, 235102.
[20] L. Chua, *Appl. Phys. A* **2011**, *102*, 765.
[21] L. O. Chua, *Proc. IEEE* **2012**, *100*, 1920.
[22] M. P. Sah, H. Kim, L. Chua, *IEEE Circuits and Systems Magazine* **2013**, *13*, in press.
[23] M. D. Pickett, G. Medeiros-Ribeiro, R. S. Williams, *Nat. Mater.* **2012**, *12*, 114.
[24] M. D. Ventra, Y. V. Pershin, L. Chua, *Proc. IEEE* **2009**, *97*, 1717.
[25] A. C. Keefe, G. P. Carman, *Smart Mater. Struct.* **2000**, *9*, 665.
[26] J. Kim, B. Kang, *Smart Mater. Struct.* **2001**, *10*, 750.
[27] Y. Fang, T. J. Pence, X. Tan, *IEEE/ASME Trans. Mechatron.* **2011**, *16*, 656.
[28] X. Chen, S. Zhang, D. A. Dikin, W. Ding, R. S. Ruoff, L. Pan, Y. Nakayama, *Nano Lett.* **2003**, *3*, 1299.
[29] P. X. Gao, W. Mai, Z. L. Wang, *Nano Lett.* **2006**, *6*, 2536.
[30] L. Chua, V. Sbitnev, H. Kim, *Int. J. Bifurcation Chaos* **2012**, *22*, 1230011.

Supporting Information

Click here to download Supporting Information: Movie S1.wmv

Fig1

Fig2

Fig3

Fig4

FigTOC

Click here to download Production Data: TOC.doc